We are IntechOpen,
the world's leading publisher of
Open Access books
Built by scientists, for scientists

6,900
Open access books available

185,000
International authors and editors

200M
Downloads

154
Countries delivered to

Our authors are among the

TOP 1%
most cited scientists

12.2%
Contributors from top 500 universities

CLARIVATE ANALYTICS
BOOK CITATION INDEX
INDEXED

WEB OF SCIENCE™

Selection of our books indexed in the Book Citation Index
in Web of Science™ Core Collection (BKCI)

Interested in publishing with us?
Contact book.department@intechopen.com

Time Modulated Linear Array (TMLA) Design

Oussama Gassab, Arab Azrar and Sara Bouguerra

Abstract

In this chapter, time modulated linear array (TMLA) is presented and discussed in detail where all its theoretical backgrounds are derived. The difference between single and multiple time modulation frequencies of TMLA is shown, where different examples in designing them are presented. In addition, the power and directivity of TMLAs are derived in their closed form. Moreover, the relation between the steering angle of each sideband with respect to the first sideband angle is developed analytically. Also, an efficient mathematical method is presented to design TMLA with desired sidelobe (SLL) and sideband levels (SBLs) with maximum attainable directivity. It is shown that the TMLA can be designed by only controlling its time sequence distributions which is a very good advantage as compared to the conventional antenna array.

Keywords: antenna array, time modulated linear array (TMLA), time modulation, power radiation, directivity, sidelobe level (SLL), sideband level (SBL), electronic beam steering, single time modulation frequency, multiple time modulation frequency

1. Introduction

The antenna array performance can be improved by decreasing its sidelobe level (SLL) and increasing its directivity. To do that, many different methods and techniques were proposed such as genetic algorithm (GA), particle swarm optimization (PSO), and hybridization between different arrays [1–3]. However, these methods provide very satisfactory results in the designed array; the realization of the designed excitations by using conventional approaches, such as tapered amplitude distributions and amplitude attenuators, is very challenging due to the fact that any small inaccuracy in the design will cause unwanted deviations in the SLL [4]. In order to overcome this problem, the time modulated linear array (TMLA), also called 4-D antenna array, was proposed. The main concept of this idea was used in [5] and applied to antenna array in order to achieve ultralow sidelobe level by Kummer et al in [6]. The idea of TMLA is to use the time as an additional degree of freedom in the design by using radio-frequency switches that periodically modulate the elements. The concept of TMLA is to use switching modulation (on, off) in order to reduce the effects of errors because the on-off switching can be controlled at a very high accuracy level.

2. Time modulated linear array

Suppose an N-isotropic element 4-D linear array aligned along the z-axis and centered on its origin as shown in **Figure 1**.

The array factor of time modulated array is given by [7]

$$\text{AF}(\theta, t) = e^{j2\pi f_0 t} \sum_n I_n g_n(t) e^{jkz_n \cos(\theta)} \tag{1}$$

where f_0 is the center frequency; θ is the elevation angle of the usual spherical coordinate; I_n are the time-independent static excitation amplitude; $k = 2\pi/\lambda$ is the wavenumber, in which λ is the wavelength; and z_n is the position of the nth element of the array along the z-axis.

2.1 TMLA with single time modulation frequency (STMF)

$g_n(t)$ are the periodic switch-on time sequence functions, and they are written for the case of STMF as [7] (see **Figure 2**)

$$g_n(t) = \begin{cases} 1, & t_{\text{on},n} < t \leq t_{\text{off},n} \\ 0, & 0 < t \leq t_{\text{on},n} \text{ or } t_{\text{off},n} < t \leq T_p \end{cases} \tag{2}$$

It should be indicated that in the STMF, the switching period T_p is the same for all the antenna elements.
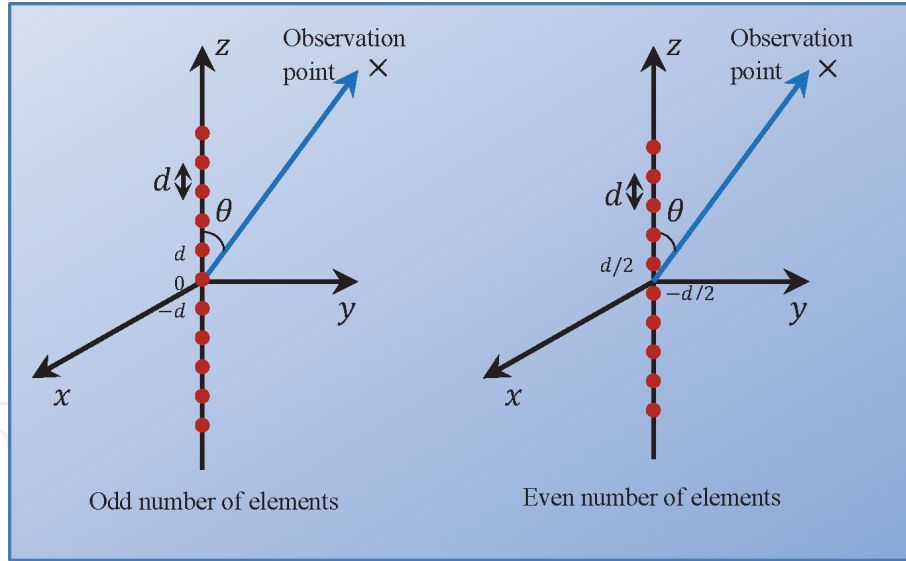

Figure 1.
Time modulated array elements positions aligned along the z-axis and centered on its origin.
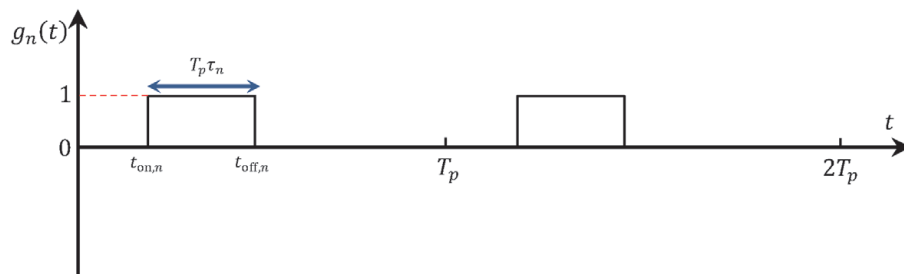

Figure 2.
The periodic time sequence graph.

The topology of TMLA with STMF is shown in **Figure 3**, where single-throw switches are connected to each antenna so that to control the switching between the two states: on and off.

Since $g_n(t)$ are periodic functions, they can be expanded by the Fourier series as

$$g_n(t) = \sum_{m=-\infty}^{+\infty} G_{nm} e^{j2\pi m f_p t} \tag{3}$$

where $f_p = 1/T_p$ is the modulation frequency, $f_0 \gg f_p$, and G_{nm} is the mth Fourier coefficient of the nth radio-frequency switch, and they are represented as

$$G_{nm} = \frac{1}{T_p} \int_0^{T_p} g_n(t) e^{-j2\pi m f_p t} dt \tag{4}$$

$$G_{nm} = \tau_n \mathrm{sinc}(\tau_n m) e^{-jm\pi(2\xi_{\mathrm{on},n}+\tau_n)} \tag{5}$$

where $\tau_n = (t_{\mathrm{off},n} - t_{\mathrm{on},n})/T_p$ and $\xi_{\mathrm{on},n} = t_{\mathrm{on},n}/T_p$ are the normalized switch-on duration and the normalized switch-on instant, respectively, and $\mathrm{sinc}(x) = \sin(\pi x)/\pi x$, wherein $\mathrm{sinc}(0) = 1$. By using (3), equation (1) can be written as

$$\mathrm{AF}(\theta,t) = \sum_{m=-\infty}^{+\infty} \sum_n I_n G_{nm} e^{j2\pi(f_0+mf_p)t} e^{jkz_n \cos(\theta)} \tag{6}$$

$$\mathrm{AF}(\theta,t) = \sum_{m=-\infty}^{+\infty} AF_m(\theta,t) \tag{7}$$

where

$$\mathrm{AF}_m(\theta,t) = \sum_n I_n G_{nm} e^{j2\pi(f_0+mf_p)t} e^{jkz_n \cos(\theta)} \tag{8}$$

Note that $\mathrm{AF}_0(\theta,t)$ is the array factor at the desired frequency f_0 and $\mathrm{AF}_m(\theta,t)$ is the sideband array factor for the case of STMF.

The array factor at the desired frequency f_0 and for the case $I_n = 1$ is given as

$$\mathrm{AF}_0(\theta,t) = e^{j2\pi f_0 t} \sum_n \tau_n e^{jkz_n \cos(\theta)}, 0 \leq \tau_n \leq 1 \tag{9}$$
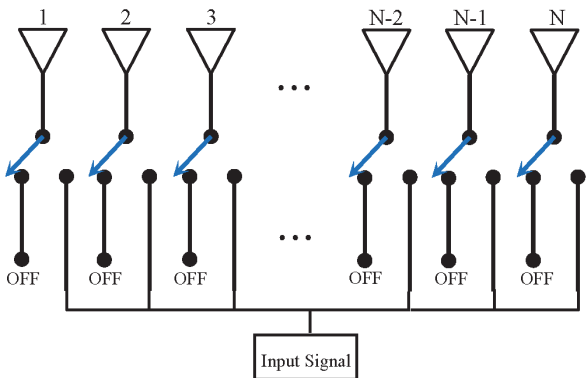

Figure 3.
Configuration of N-element TMLA with STMF using single-throw switches.

It can be concluded that by controlling the normalized switch-on durations τ_n, any array pattern AF_0 can be generated with very high accuracy.

2.1.1 Power radiations in time domain

In this section, we outline how to obtain the generalized power expression of the TMLA. By aligning the array along the z-axis and considering spherical coordinate with θ_p and ϕ_p, the elevation and azimuth angles, respectively, Eq. (1) can be represented in terms of θ_p as

$$AF(\theta_p, t) = e^{j2\pi f_0 t} \sum_{n=1}^{N} I_n g_n(t) e^{jkz_n \cos(\theta_p)} = e^{j2\pi f_0 t} \mathcal{AF}(\theta_p, t) \quad (10)$$

where z_n denotes the positions of the TMLA elements along the z-axis.

Let's consider $\vec{E}_0$ and $\vec{H}_0$ be the intensities of the electric and magnetic field (complex spatial form) radiated by a given antenna used in the TMLA, hence, the electric field and magnetic field generated by the array are given as

$$\vec{E}(t) = e^{j2\pi f_0 t} \mathcal{AF}(\theta_p, t) \vec{E}_0 \quad (11)$$

$$\vec{H}(t) = e^{j2\pi f_0 t} \mathcal{AF}(\theta_p, t) \vec{H}_0 \quad (12)$$

The instantaneous Poynting vector is given as [8]

$$\vec{\mathcal{P}} = \vec{\mathcal{E}} \times \vec{\mathcal{H}} \quad (13)$$

where $\vec{\mathcal{E}}$ and $\vec{\mathcal{H}}$ represent the instantaneous field vectors, and they are given as

$$\vec{\mathcal{E}}(t) = \mathrm{Re}\left\{ e^{j2\pi f_0 t} \mathcal{AF}(\theta_p, t) \vec{E}_0 \right\} \quad (14)$$

$$\vec{\mathcal{H}}(t) = \mathrm{Re}\left\{ e^{j2\pi f_0 t} \mathcal{AF}(\theta_p, t) \vec{H}_0 \right\} \quad (15)$$

By using $\mathrm{Re}\{X\} = (X + X^*)/2$ and inserting (14) and (15) in (13) and proceeding with the same analysis performed in [8], the following result is obtained:

$$\mathcal{P} = \frac{1}{2} \mathrm{Re}\left\{ |\mathcal{AF}|^2 \vec{E}_0 \times \vec{H}_0^* \right\} + \frac{1}{2} \mathrm{Re}\left\{ \mathcal{AF}^2 \vec{E}_0 \times \vec{H}_0 e^{j4\pi f_0 t} \right\} \quad (16)$$

Note that $\vec{E}_0$ and $\vec{H}_0$ are not functions of time and $\mathcal{AF}$ is a periodic function with period $T_p \gg T_0$, and then the second term has zero average power; hence, the average power density is equal to

$$P_{\text{density}} = \frac{W_{\text{avg}}}{T_p} \int_0^{T_p} |\mathcal{AF}|^2 dt \quad (17)$$

where $W_{\text{avg}} = \frac{1}{2} \mathrm{Re}\left\{ \vec{E}_0 \times \vec{H}_0^* \right\}$ is the power density of each antenna element in the TMLA. By considering isotropic antenna elements, $W_{\text{avg}} \, r^2$ is the radiation intensity, and it is constant over all the space, and it can be taken as unity (r is the

radial distance from the TMLA to the observation point at the far-field region). By using (1), (17) is written as

$$P_{\text{density}} = \frac{W_{\text{avg}}}{T_p} \sum_{n,k=1}^{N} I_n I_k^* \int_0^{T_p} g_n(t) g_k^*(t) dt e^{jk(z_n - z_k)\cos(\theta_p)} \tag{18}$$

The total power is given

$$P_T = \int_0^{2\pi} \int_0^{\pi} P_{\text{density}} r^2 \sin(\theta_p) d\theta_p d\phi_p = 4\pi \sum_{n,k=1}^{N} I_n I_k^* \frac{1}{T_p} \int_0^{T_p} g_n(t) g_k^*(t) dt \operatorname{sinc} \frac{2}{\lambda}(z_n - z_k) \tag{19}$$

We should indicate that the expression (19) is a very simple formula to determine the total power radiated by the TMLA.

For the case $d = \lambda/2$ and equal spacing distance between the elements, the total power can be written as

$$P_T = 4\pi \sum_{n=1}^{N} |I_n|^2 \frac{1}{T_p} \int_0^{T_p} g_n(t)^2 dt = 4\pi \sum_{n=1}^{N} |I_n|^2 \tau_n \tag{20}$$

2.1.2 Power radiations in frequency domain

In this section, the power radiation is represented in the frequency domain. By taking the Fourier series (3) of $g_n(t)$ and using the Parseval's theorem then

$$\frac{1}{T_p} \int_0^{T_p} g_n(t) g_k^*(t) dt = \sum_{m=-\infty}^{+\infty} G_{nm} G_{km}^* \tag{21}$$

and the total power is given as

$$P_T = 4\pi \sum_{n,k=1}^{N} I_n I_k^* \sum_{m=-\infty}^{+\infty} G_{nm} G_{km}^* \operatorname{sinc} \frac{2}{\lambda}(z_n - z_k) \tag{22}$$

It is worth noticing that the total power P_T can be written as

$$P_T = P_{f_0} + P_{SB} \tag{23}$$

and

$$P_{f_0} = 4\pi \sum_{n=1}^{N} |I_n|^2 \tau_n^2 + 4\pi \sum_{\substack{n,k=1 \\ k \neq n}}^{N} I_n I_k^* \operatorname{sinc} \frac{2}{\lambda}(z_n - z_k) \tau_n \tau_k \tag{24}$$

$$P_{SB} = 4\pi \sum_{n=1}^{N} |I_n|^2 \sum_{\substack{m=-\infty \\ m \neq 0}}^{+\infty} |G_{nm}|^2 + 4\pi \sum_{\substack{n,k=1 \\ k \neq n}}^{N} I_n I_k^* \operatorname{sinc} \frac{2}{\lambda}(z_n - z_k) \sum_{\substack{m=-\infty \\ m \neq 0}}^{+\infty} G_{nm} G_{km}^* \tag{25}$$

where P_{f_0} is the power radiated at the fundamental frequency f_0 and P_{SB} is the power of sidebands.

The complex Fourier coefficient G_{nm} in (5) can be written as

$$G_{nm} = \frac{j}{2\pi m}\left(e^{-j2\pi m\xi_{\text{off},n}} - e^{-j2\pi m\xi_{\text{on},n}}\right) \tag{26}$$

Then

$$G_{nm}G_{km}^* = \frac{1}{4\pi^2 m^2}\left[e^{j2\pi m\left(\xi_{\text{off},k}-\xi_{\text{off},n}\right)} - e^{j2\pi m\left(\xi_{\text{on},k}-\xi_{\text{off},n}\right)} - e^{j2\pi m\left(\xi_{\text{off},k}-\xi_{\text{on},n}\right)} + e^{j2\pi m\left(\xi_{\text{on},k}-\xi_{\text{on},n}\right)}\right] \tag{27}$$

Then, we have

$$\sum_{\substack{m=-\infty \\ m\neq 0}}^{+\infty} G_{nm}G_{km}^* = \left[2\sum_{m=1}^{+\infty}\frac{\cos 2\pi m\left(\xi_{\text{off},k}-\xi_{\text{off},n}\right)}{(2\pi m)^2} - 2\sum_{m=1}^{+\infty}\frac{\cos 2\pi m\left(\xi_{\text{on},k}-\xi_{\text{off},n}\right)}{(2\pi m)^2}\right.$$
$$\left. -2\sum_{m=1}^{+\infty}\frac{\cos 2\pi m\left(\xi_{\text{off},k}-\xi_{\text{on},n}\right)}{(2\pi m)^2} + 2\sum_{m=1}^{+\infty}\frac{\cos 2\pi m\left(\xi_{\text{on},k}-\xi_{\text{on},n}\right)}{(2\pi m)^2}\right] \tag{28}$$

By using the results given in [9], then

$$\sum_{\substack{m=-\infty \\ m\neq 0}}^{+\infty} G_{nm}G_{km}^* = \bar{\tau}_{nk} - \tau_n\tau_k \tag{29}$$

where

$$\bar{\tau}_{nk} = \frac{1}{2}\left(-\left|\xi_{\text{off},k}-\xi_{\text{off},n}\right| + \left|\xi_{\text{on},k}-\xi_{\text{off},n}\right| + \left|\xi_{\text{off},k}-\xi_{\text{on},n}\right| - \left|\xi_{\text{on},k}-\xi_{\text{on},n}\right|\right) \tag{30}$$

It should be indicated that $\bar{\tau}_{nk}$ can be interpreted as the overlapped duration between the corresponding switch-on durations τ_n and τ_k.

At the case $n = k$, the Parseval's theorem (21) can be used, then

$$\sum_{\substack{m=-\infty \\ m\neq 0}}^{+\infty} |G_{nm}|^2 = \frac{1}{T_p}\int_0^{T_p} |g_n(t)|^2 dt - |G_{n0}|^2 \tag{31}$$

and

$$\sum_{\substack{m=-\infty \\ m\neq 0}}^{+\infty} |G_{nm}|^2 = \tau_n(1-\tau_n) \tag{32}$$

It should be indicated that (29) and (32) can be used in (25) in order to obtain the closed-form expression for the sideband power.

It is worth noticing that the total power expression (22) can be written as

$$P_T = 4\pi \sum_{n,k=1}^{N} I_n I_k^* \bar{\tau}_{nk} \mathrm{sinc} \frac{2}{\lambda}(z_n - z_k) \tag{33}$$

2.1.3 Directivity

The directivity at the fundamental frequency f_0 of TMLA with STMF is presented as [10]

$$D_{f_0} = \frac{4\pi |AF_0(\theta,t)_{\max}|^2}{P_T} \tag{34}$$

By considering excitations with the same amplitude, i.e., $I_n = 1$ as shown in Eq. (9), the directivity D_{f_0} can be written as

$$D_{f_0} = \frac{4\pi \left|\sum_n \tau_n\right|^2}{P_{f_0}} \frac{P_{f_0}}{P_{f_0} + P_{SB}} \tag{35}$$

It can be written in the following form [10]:

$$D_{f_0} = D_{\mathrm{conv}} \eta_{f_0} \tag{36}$$

where $D_{\mathrm{conv}} = 4\pi \left|\sum_n \tau_n\right|^2 / P_{f_0}$ is the directivity of the conventional antenna array, i.e., without modulation switches, and η_{f_0} is the dynamic factor. It is worth noticing that $\eta_{SB} = 1$ denotes no sideband radiations (SBRs).

2.1.4 Simulation and computed results

To understand the benefits of TMLA with STMF, simulation examples should be analyzed in detail. Let's consider 30-element Chebyshev weighting with 30 dB SLL, where $I_n = 1$ is considered. The normalized array pattern at the fundamental frequency and the first four sidebands frequencies are shown in **Figure 4**, whereas the periodic time sequences for each element are shown in **Figure 5**. It is evident that the array pattern at the fundamental frequency has a Chebyshev array pattern. However, there are other array patterns at the multiple of the time modulation frequency f_p due to the modulating switches, which cause power losses at the SBRs. The power distribution over the sidebands is shown in **Figure 6**, where only the positive sidebands are shown because the negative sidebands have the same power distribution as the positive ones.

It is evident that most of the power resides at the fundamental frequency f_0 with 75.94%, where the remaining sidebands have only 24.06% of the total power. It should be indicated that the directivity of the array pattern at the fundamental frequency f_0 is equal to 19.93 dBi which is less than the conventional array directivity 26.24 dBi because of the SBR losses. Many wondering facts may arise now; since the conventional array has no sideband power losses and higher directivity than the TMLA, why is the TMLA really needed? Why do we need modulating switches that generate infinite sideband at the multiple of the modulation frequency? The answer is simple; the conventional array needs tapered amplitude
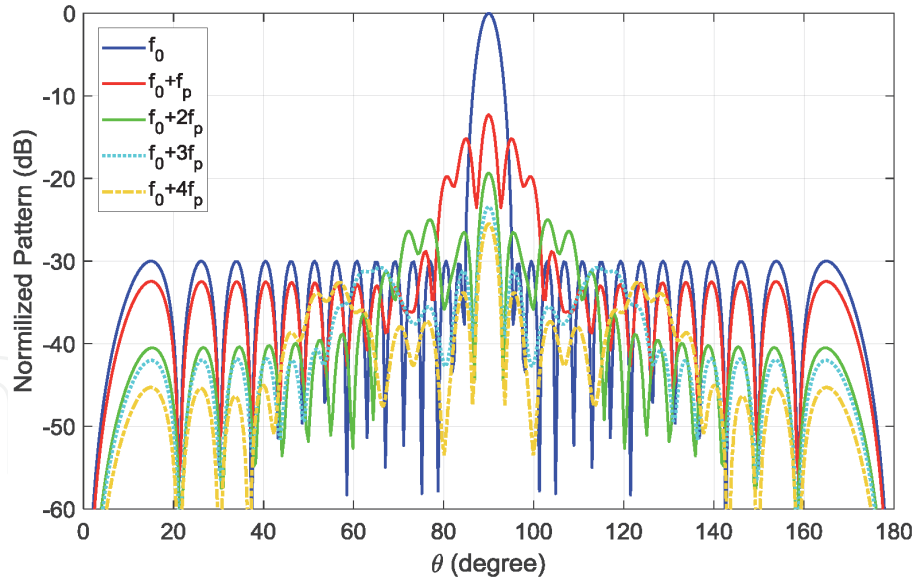
Figure 4.
The array patterns of TMLA with Chebyshev weighting at the fundamental frequency and the four positive first sidebands.
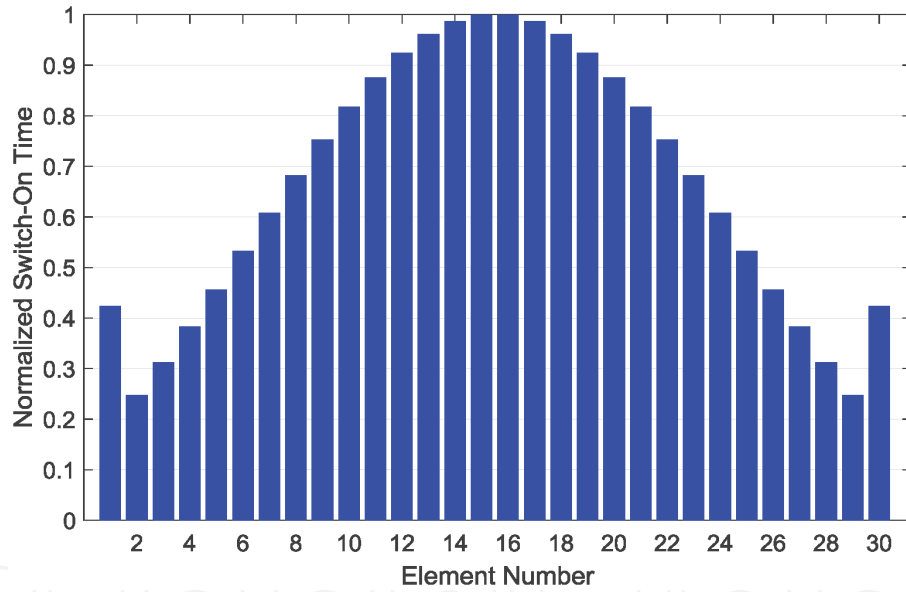

Figure 5.
The periodic time sequences of each element of TMLA, where all the switch-on instants are equal to zero.

distributions and amplitude attenuators [4] in order to realize the excitation amplitudes. However, this method is not so accurate; hence, it causes deviations in the desired array pattern. Therefore, high SLLs are generated. In this case, the realistic directivity is dramatically reduced. Whereas the excitation amplitudes in TMLA can be easily generated with very high accuracy by using modulating switches, therefore, the desired array pattern is totally preserved (its SLLs are kept at their designed level).

It is worth noticing that the sideband levels (SBLs) are high at the main lobe of the fundamental array pattern as shown in **Figure 4**. This kind of problem can be solved by shifting the sideband arrays by controlling the normalized switch-on instants $\xi_{on,n}$.

The array factor at the mth sideband for static excitation amplitude $I_n = 1$ and equal spacing distance between the elements ($z_n = (n-1)d$) is given by (8)
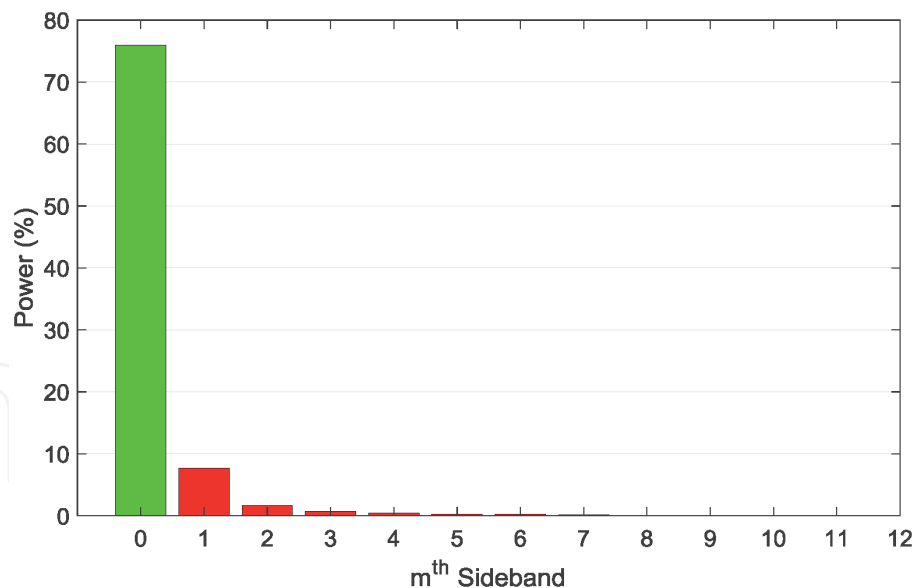
Figure 6.
Power percentage spectrum of TMLA (Chebyshev weighting with N = 30 and SLL= −30 dB).

$$\text{AF}_m(\theta, t) = e^{j2\pi \left(f_0 + mf_p \right)t} \sum_{n=1}^{N} \tau_n \text{sinc}(\tau_n m) e^{j\left(-m\pi \left(2\xi_{\text{on},n} + \tau_n \right) + k(n-1)d \cos(\theta) \right)} \tag{37}$$

Without steering the mth sideband, the switch-on instant is zero $\xi_{\text{on},n} = 0$ then $-m\pi \left(2\xi_{\text{on},n} + \tau_n \right) = -m\pi\tau_n$, which represent an original phase shift at the mth sideband. Hence, (37) can be written as

$$\text{AF}_m(\theta, t) = e^{j2\pi \left(f_0 + mf_p \right)t} \sum_{n=1}^{N} \tau_n \text{sinc}(\tau_n m) e^{-m\pi\tau_n} e^{j\left(-2m\pi\xi_{\text{on},n} + k(n-1)d \cos(\theta) \right)} \tag{38}$$

To steer the mth sideband toward θ_0, the following condition should be taken

$$e^{j\left(-2m\pi\xi_{\text{on},n} + k(n-1)d \cos(\theta) \right)} = 1 \tag{39}$$

The general solution of Eq. (39) is given as

$$\xi_{\text{on},n} = \frac{k(n-1)d}{2\pi m} \cos(\theta_0) + \frac{\mathcal{K}}{m}, \qquad \mathcal{K} \in \mathbb{Z} \tag{40}$$

We should indicate that $\mathcal{K}$ is an integer number which is chosen in order to maintain $\xi_{\text{on},n}$ in the region $[0, 1]$. It should be indicated that when the first sideband is steered toward θ_0, i.e., $m = 1$ at relation (40), the mth sideband is self-steered toward a specific angle θ_m that can be determined as

By substituting (40) with $m = 1$ in (38), the following relation is obtained

$$\text{AF}_m(\theta, t) = e^{j2\pi \left(f_0 + mf_p \right)t} \sum_{n} \tau_n \text{sinc}(\tau_n m) e^{-m\pi\tau_n} e^{j(n-1)(-kmd \cos(\theta_0) + kd \cos(\theta))} \tag{41}$$

To find θ_m, the following equation should be solved

$$e^{j(n-1)(-kmd \cos(\theta_0) + kd \cos(\theta))} = 1 \tag{42}$$

9

Its general solution is given as

$$\theta_m = \arccos\left(m\cos\left(\theta_0\right) + 2\mathcal{K}\right), \qquad \mathcal{K} \in \mathbb{Z} \tag{43}$$

It should be indicated that if $|m\cos\left(\theta_0\right)| > 1$, then $\mathcal{K}$ is chosen from $\mathbb{Z}$ (integer numbers set) so that $|m\cos\left(\theta_0\right) + 2\mathcal{K}| \leq 1$. For example, let steer the first sideband toward $\theta_0 = 120°$, then the 2nd, 3rd, and 4th sidebands are steered toward $180°, 60°$, and $90°$, respectively. The results are shown in **Figure 7** (a), where the corresponding switch-on time is shown in **Figure 7** (b). When the first sideband is steered toward $\theta_0 = 180°$, then the 2nd, 3rd, and 4th sidebands are steered toward $90°, 180°$, and $90°$, respectively. The normalized array pattern is shown in **Figure 8** (a), and the corresponding switch-on time for each antenna element is presented in **Figure 8** (b). We should indicate that the even sidebands, i.e., m is even, are not
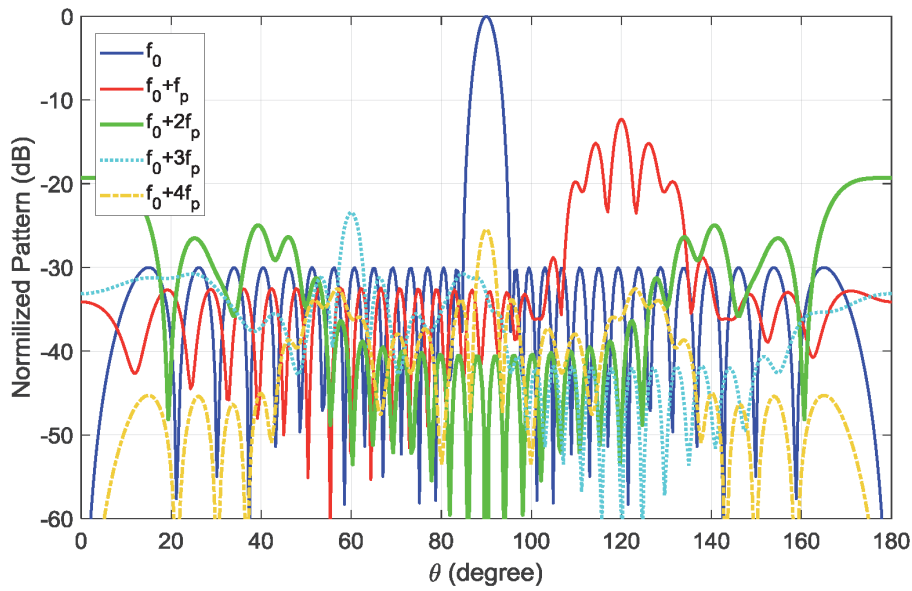
(a)
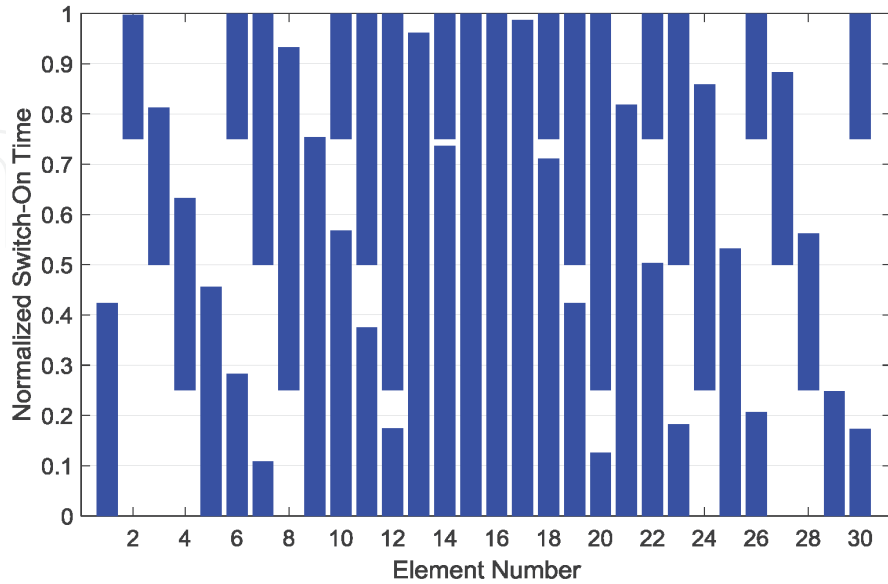
(b)

Figure 7.
(a) The array patterns of TMLA with Chebyshev weighting at the fundamental frequency and steered four positive sidebands where the first positive side is steered toward 120°. (b) The periodic time sequences of each element of TMLA.
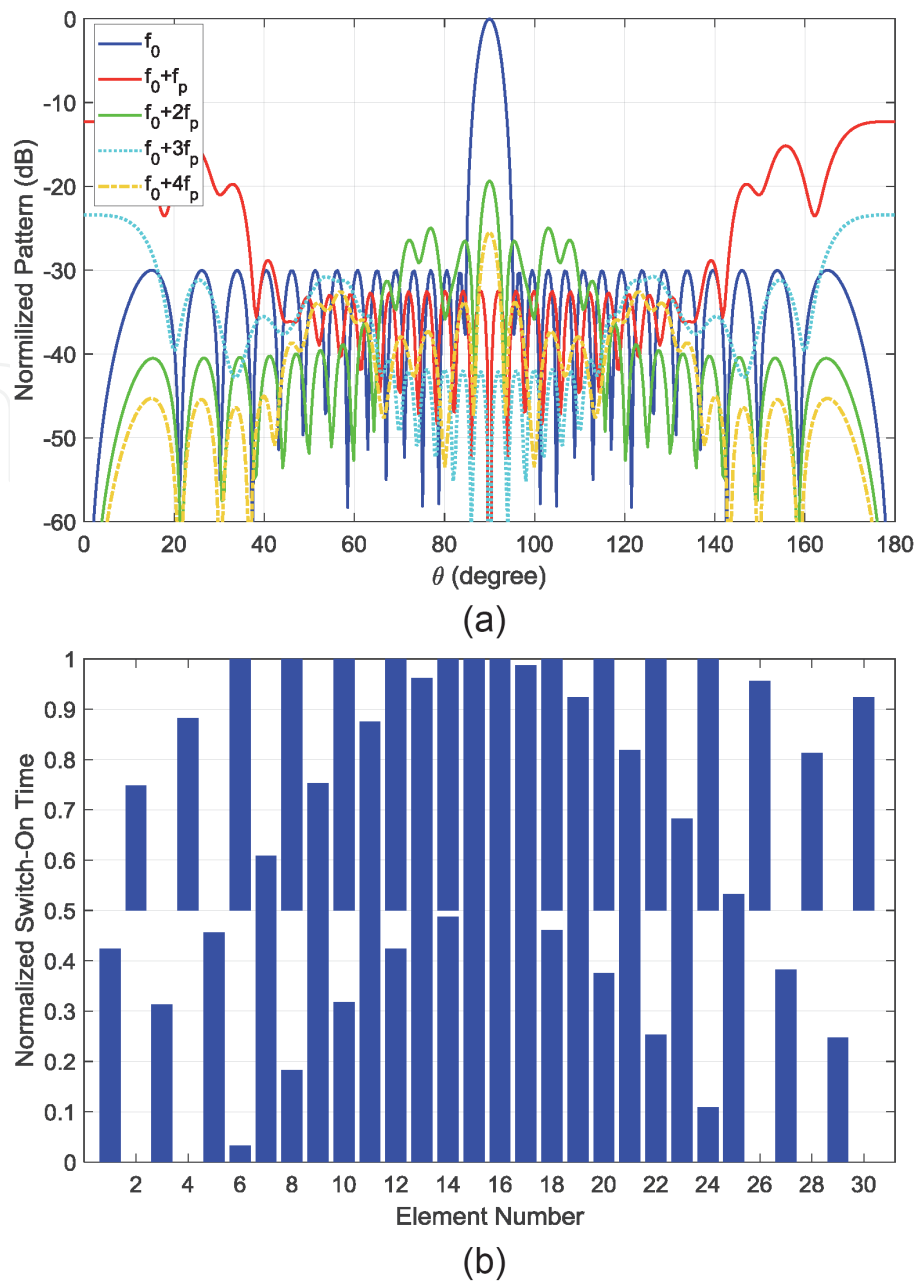
Figure 8.
(a) The array patterns of TMLA with Chebyshev weighting at the fundamental frequency and steered four positive sidebands where the first positive side is steered toward 180°. (b) The periodic time sequences of each element of TMLA.

steered at the case $\theta_0 = 180°$ because there exists an integer number $\mathcal{K} \in \mathbb{Z}$ so that $-m + 2\mathcal{K} = 0$ in Eq. (43). It is worth noticing that the power distribution over the sidebands as given in **Figure 6** remains unchanged for all the steering angles.

From the above results, it can be deduced that the use of periodic switches to modulate the signal generates SBRs at the multiples of the time modulation frequency, which causes power loss and low directivity. To overcome the SBR problem, the optimization techniques, such as differential evolution (DE), GA, PSO, and the simulated annealing (SA), were used to reduce the SBL as well as maintain SLL at a certain low level [11–14]. In [14], the PSO technique was used in order to minimize the power losses and maintain the SLL and SBL at the desired level; therefore the time sequences generated by the PSO are given in **Figure 9**, and the corresponding array pattern is presented in **Figure 10**.

It can be observed that the SLLs are maintained at −20 dB and the maximum SBL is −30.2 dB, where only four elements are time modulated and the elements 1,
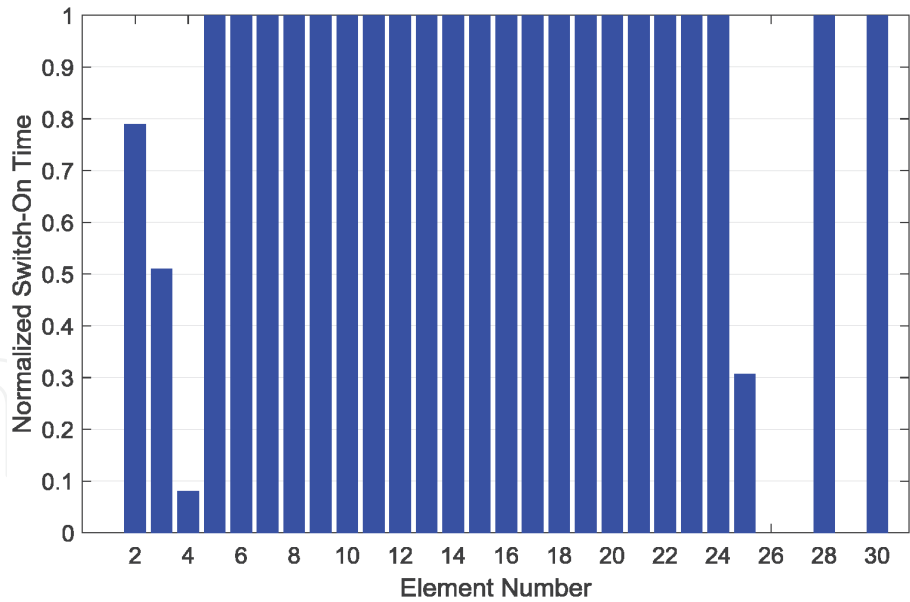
Figure 9.
Switch-on time sequences optimized by PSO technique in order to reduce the SBR (N = 30, d = 0.7λ) [13].
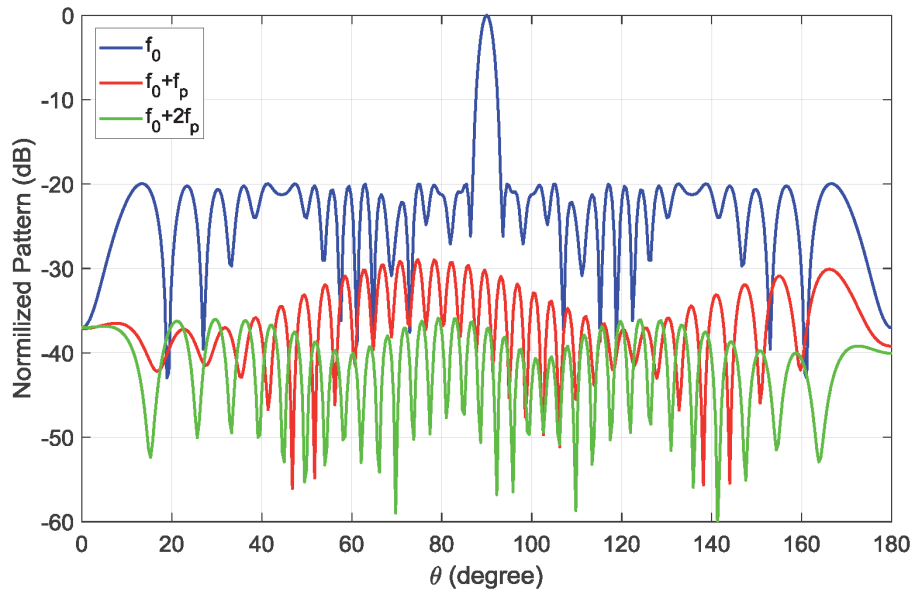

Figure 10.
Normalized array patterns (at the fundamental frequency and the two first sidebands) of the optimized TMLA by the PSO technique [13].

26, 27, and 29 are always turned off. This TMLA can be considered 26-element array with nonuniform spacing because the 4-turned off elements can be ignored. The power distribution over the sidebands is shown in **Figure 11**. It can be observed that most of the power resides at the fundamental frequency with 96.43% of the total power, where the remaining sidebands have only 3.57% of the total power. However, in this case, the SLL is only −20 dB.

In [14], the SA method was used in order to maintain the SLL at a certain level and minimize the SBL under −30 dB. Therefore, the obtained switch-on time sequences are shown in **Figure 12**, and the corresponding array patterns of the optimized TMLA are shown in **Figure 13**, where the power spectrum percentage is presented in **Figure 14**. It can be observed that only 9 elements are time modulated, where the remaining 21 elements are always turned on. In this case, the SBLs are minimized greatly, where they have only 3.96% of the total power. The PSO is more
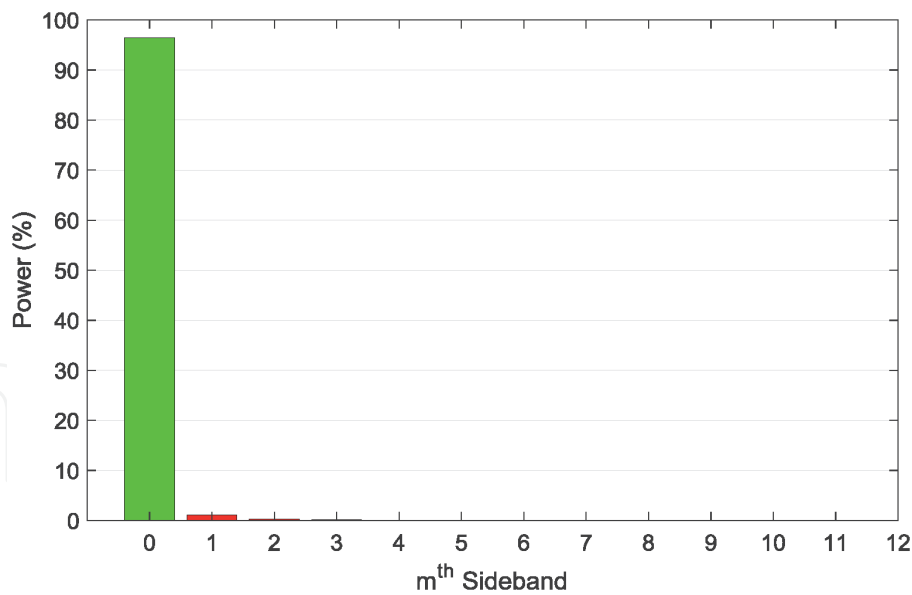
Figure 11.
Power percentage spectrum of the optimized TMLA by the PSO ($N = 30, d = 0.7\lambda$).
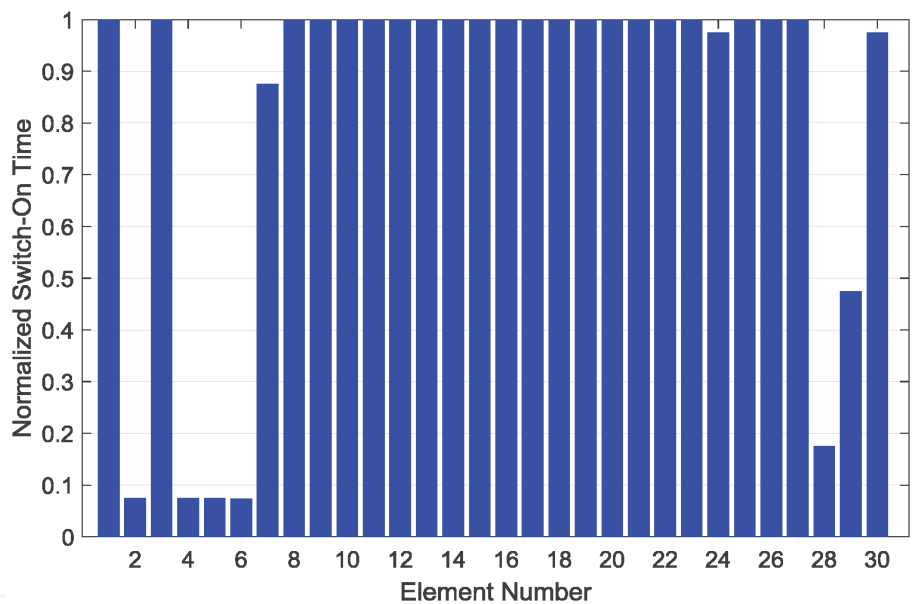

Figure 12.
Switch-on time sequences optimized by the SA technique in order to reduce the SBR ($N = 30, d = 0.7\lambda$) [14].

efficient than the SA one as indicated in [14]. For more details about the optimization methods, the reader should be referred to [13, 14].

The multiple time modulation frequency (MTMF) was proposed to reduce SBL of TMLA because of avoiding the accumulation of the sidebands in the space [15]; however, the SBR power was not decreased by using MTMF. In [16], the DE was used with MTMF to suppress SLL, SBL, and SBR power, and very good results were obtained. In the following section, the MTMF is investigated in detail.

2.2 TMLA with multiple time modulation frequency (MTMF)

In TMLA with MTMF, each antenna element has its time modulating switching period $T_{p,n}$. Hence, the periodic function $g_n(t)$ in (1) is expressed as [15]
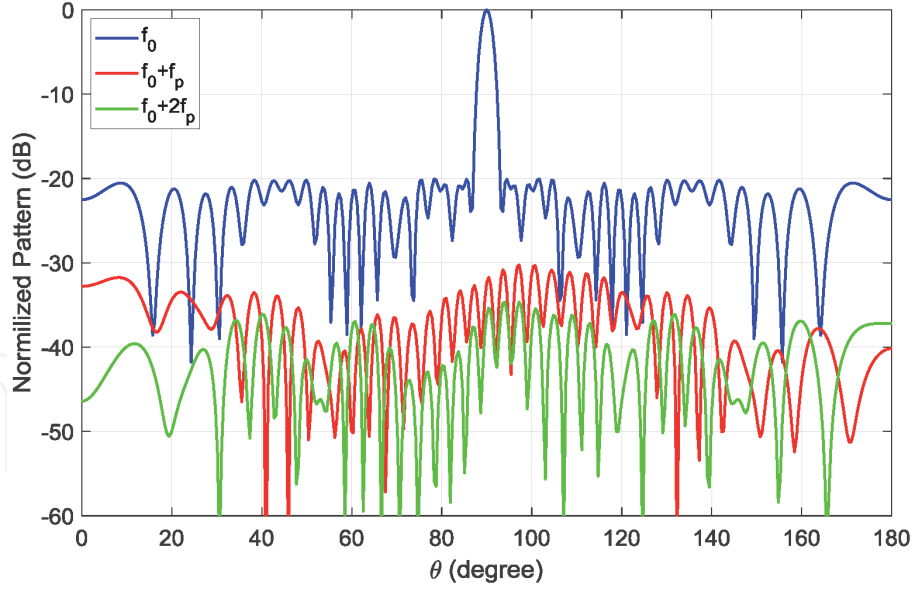
Figure 13.
Normalized array patterns (at the fundamental frequency and the two first sidebands) of the optimized TMLA by the SA technique [14].
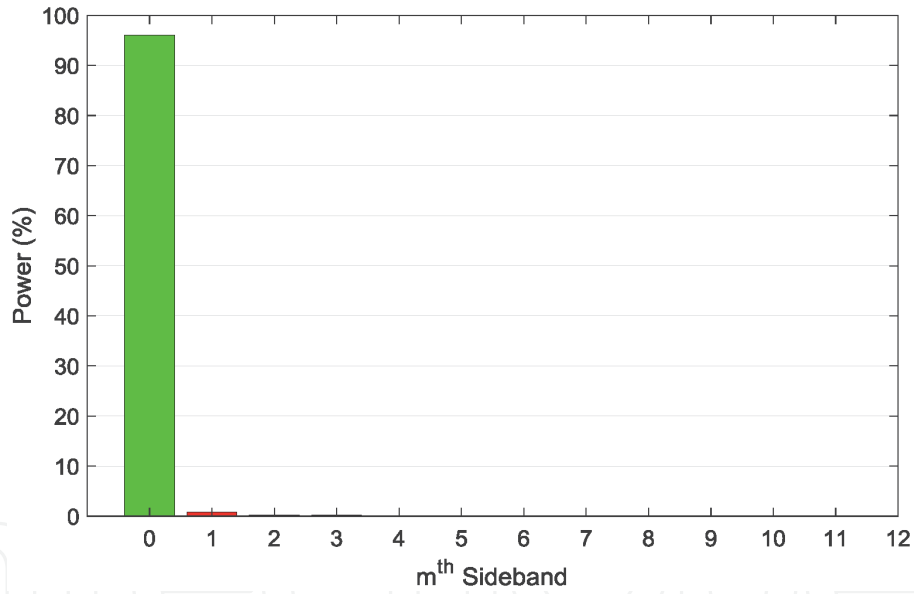

Figure 14.
Power percentage spectrum of the optimized TMLA by the SA method (N = 30, d = 0.7λ).

$$g_n(t) = \begin{cases} 1, & t_{\text{on},n} < t \leq t_{\text{off},n} \\ 0, & 0 < t \leq t_{\text{on},n} \text{ or } t_{\text{off},n} < t \leq T_{\text{p},n} \end{cases} \tag{44}$$

Since $g_n(t)$ are periodic functions, they can be expanded by the Fourier series as

$$g_n(t) = \sum_{m=-\infty}^{+\infty} G_{nm} e^{j2\pi m f_{\text{pn}} t} \tag{45}$$

where $f_{pn} = 1/T_{pn}$ is the modulation frequency and G_{nm} is the mth Fourier coefficient of the nth radio-frequency switch, and they are represented as

$$G_{nm} = \frac{1}{T_{pn}} \int_0^{T_{pn}} g_n(t) e^{-j2\pi m f_{pn} t} dt \tag{46}$$

$$G_{nm} = \tau_n \mathrm{sinc}(\tau_n m) e^{-jm\pi\left(2\xi_{on,n} + \tau_n\right)} \tag{47}$$

where $\tau_n = (t_{off,n} - t_{on,n})/T_{pn}$ and $\xi_{on,n} = t_{on,n}/T_{pn}$ are the normalized switch-on duration and the normalized switch-on instant for each element in the TMLA, respectively.

In the case of MTMF, the array factor can be written as

$$AF(\theta, t) = \sum_{m=-\infty}^{+\infty} \sum_n I_n G_{nm} e^{j2\pi\left(f_0 + m f_{pn}\right)t} e^{jkz_n \cos(\theta)} \tag{48}$$

$$AF(\theta, t) = \sum_{m=-\infty}^{+\infty} AF_m(\theta, t) \tag{49}$$

where

$$AF_m(\theta, t) = \sum_n I_n G_{nm} e^{j2\pi\left(f_0 + m f_{pn}\right)t} e^{jkz_n \cos(\theta)} \tag{50}$$

It is worth noticing that AF_0 is the array factor at the fundamental frequency f_0 and AF_m accumulates different sideband frequencies as it was described in [15, 16]. The idea of using MTMF is to avoid the superposing of sidebands because each array element has its corresponding switching frequency. Therefore, the sidebands of each element could not be superposed with the sidebands of another element; this concept is explained clearly in **Figure 15**.

2.2.1 Power radiations

The power radiation by TMLA with MTMF can be obtained by considering the following assumption:

- The sidebands of each antenna element are not overlapped with the sidebands of the other elements.

In this case, the sidebands power is given as

$$P_{SB} = \sum_{n=1}^N |I_n|^2 \sum_{\substack{m=-\infty \\ m \neq 0}}^{+\infty} |G_{nm}|^2 \tag{51}$$

$$P_{SB} = \sum_{n=1}^N |I_n|^2 \tau_n (1 - \tau_n) \tag{52}$$

where the power radiated at the fundamental frequency is given by

$$P_{f_0} = 4\pi \sum_{n=1}^N |I_n|^2 \tau_n^2 + 4\pi \sum_{\substack{n,k=1 \\ k \neq n}}^N I_n I_k^* \mathrm{sinc} \frac{2}{\lambda} (z_n - z_k) \tau_n \tau_k \tag{53}$$
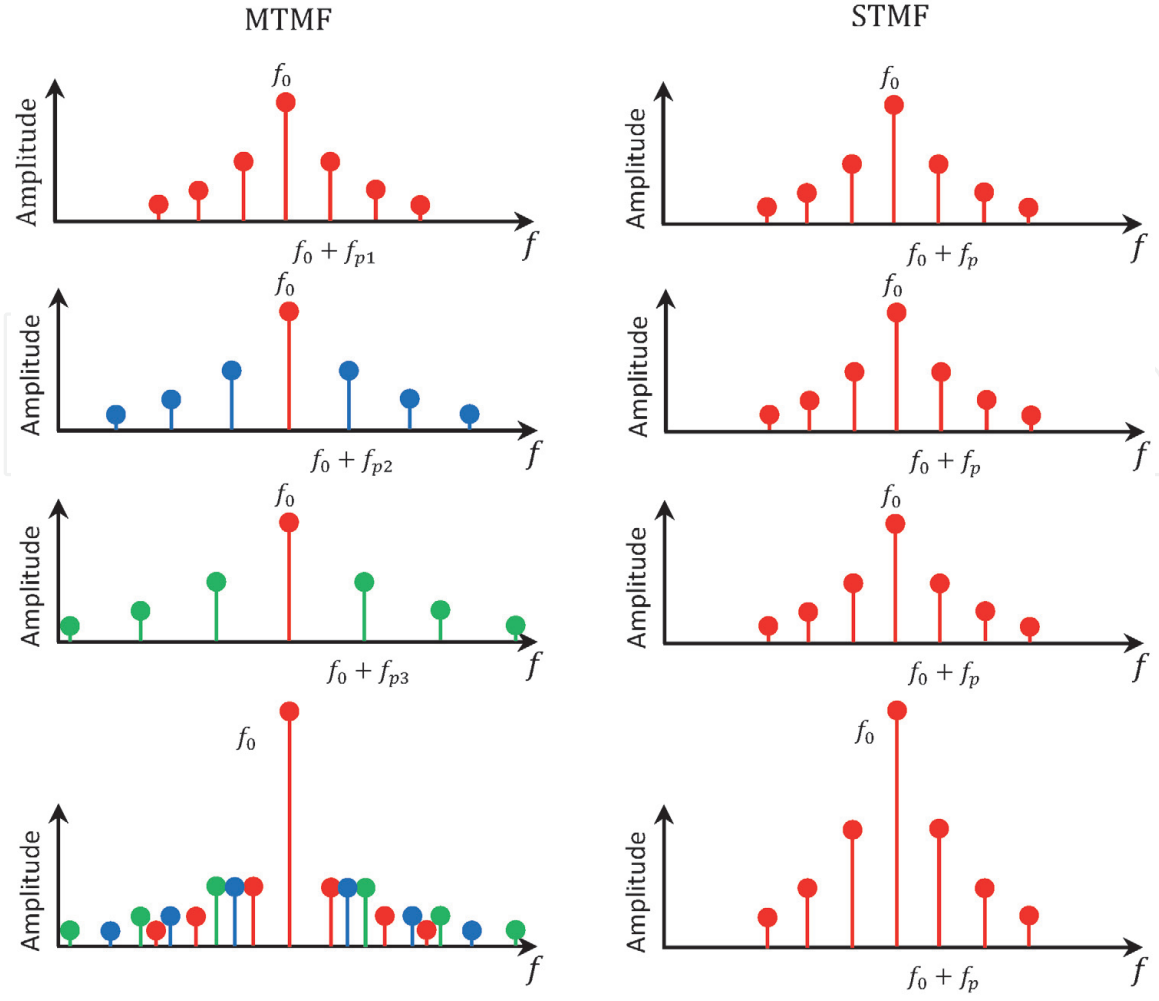
Figure 15.
Illustration of SBL suppression in TMLA with MTMF. The SBLs in STMF are superposed because all the time modulating switchers have the same time modulating frequency, whereas the SBLs in MTMF are not superposed because each element has the corresponding time modulating frequency.

It is worth noticing that relation (51) shows that all the Fourier's coefficients of each element are summed independently because they are located at different frequencies. Also, it should be indicated that for $d = \lambda/2$ the total power relations for the STMF and MTMF are identical. Another formulation for the power relation of TMLA with MTMF is given in [17], where a prime distribution is assumed for the time modulation frequencies. For more details about time modulation frequencies with prime distribution, the reader should be referred to [17]. It should be noted that the directivity of the TMLA with MTMF is identical to the one given in relation (35).

2.2.2 Simulation and computed results

In this section, computed results and examples are considered in order to investigate the benefits of TMLA with MTMF. The same example taken in Section 2.1.4 is considered so as to make a fair comparison between TMLA-STMF and TMLA-MTMF. Let's consider the fundamental frequency f_0 to be 2.6 GHz, the time modulation frequency f_p for the STMF case is 30 MHz, and for the MTMF, f_{pn} are selected as [15]

$$f_{pn} = (30 + 0.5(n - 1))\text{MHz}, \quad n = 1, 2, 3, \dots, N \tag{54}$$

The results are plotted in **Figure 16**, where the maximum sideband for the STMF is -12.28 dB, whereas only -35.98 dB is obtained for MTMF case. It is evident that
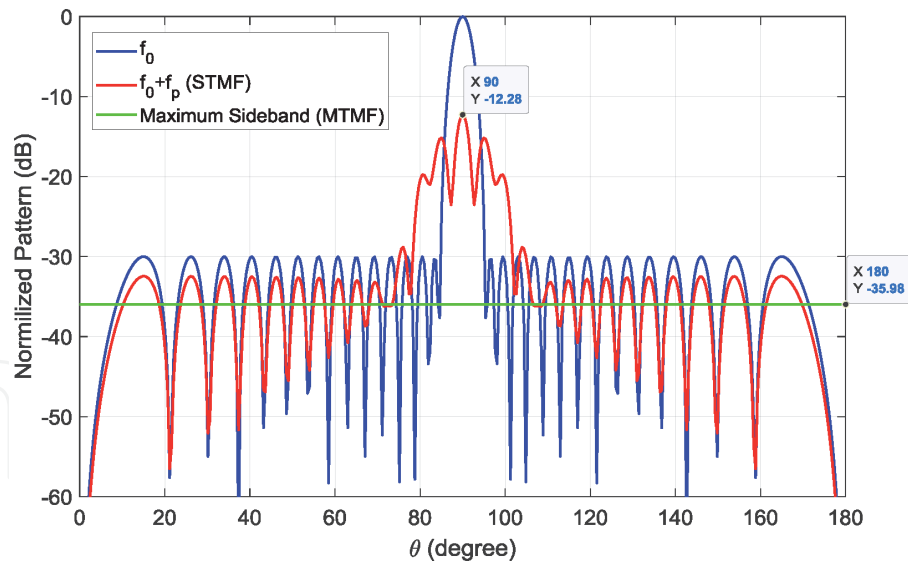
Figure 16.
Normalized array pattern at the fundamental frequency with STMF first sideband and the MTMF maximum sideband level.

the TMLA with MTMF is more efficient than STMF in reducing the sideband levels. However, the power loss in the sideband radiations is the same for the case $d = \lambda/2$; hence, the directivity has remained unchanged. It is worth noticing that the normalized switch-on time is identical to the one given in **Figure 5**, where, in the case of MTMF, each element has its corresponding normalizing period as shown in Eq. (47).

The sideband's power percentages for STMF and MTMF are presented in **Figure 17**. It is evident that the sideband's power of STMF is larger than the sideband's power of MTMF for $d/\lambda < 0.5$. However, the inverse occurs for $d/\lambda > 0.5$.

The optimization techniques were used in order to reduce the SBLs and the SBRs, e.g., the DE method was applied in [16], and very good results were obtained. In [16], the DE method was implemented so as to maintain the SLLs at a given level, whereas the SBLs and SBRs are minimized as much as possible. **Figure 18** shows the results of the DE applied to the TMLA-MTMF in order to maintain the SLLs at -20 dB, where the obtained SBL was -40.70 dB [16]. In order to make a
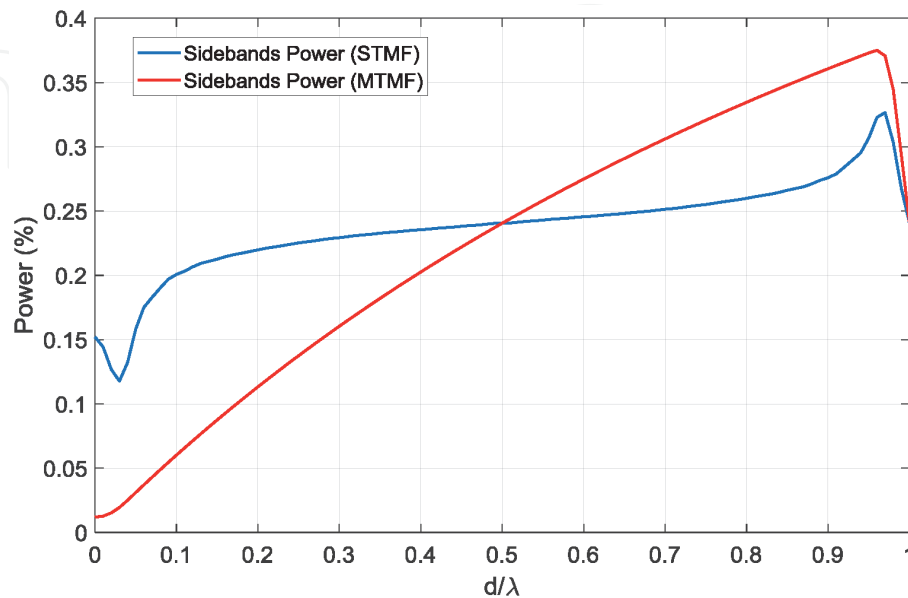

Figure 17.
Sideband's power percentage for TMLA with STMF and MTMF in terms of d/λ (Chebyshev weighting with -30 dB SLLs is considered).

(a)

(b)

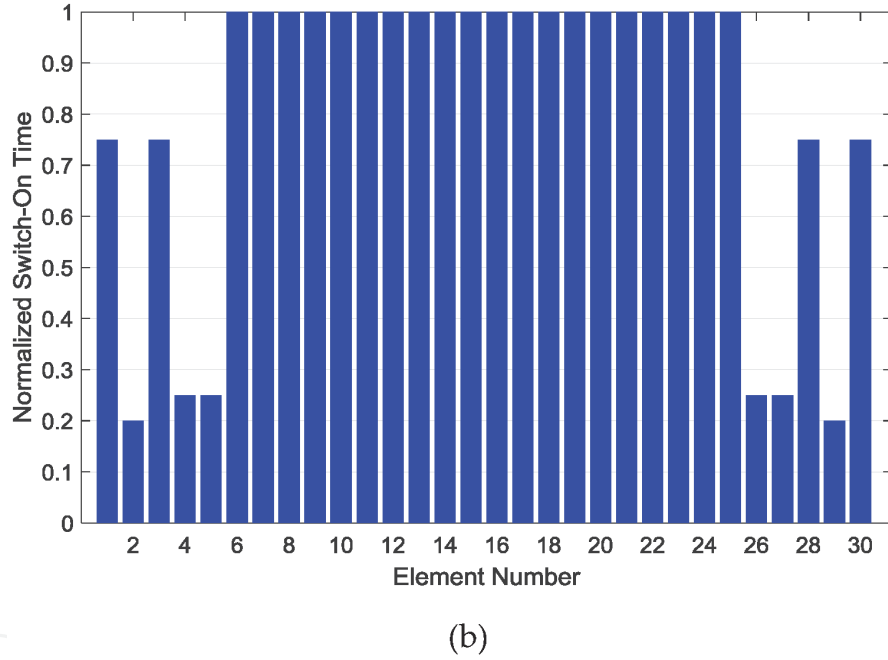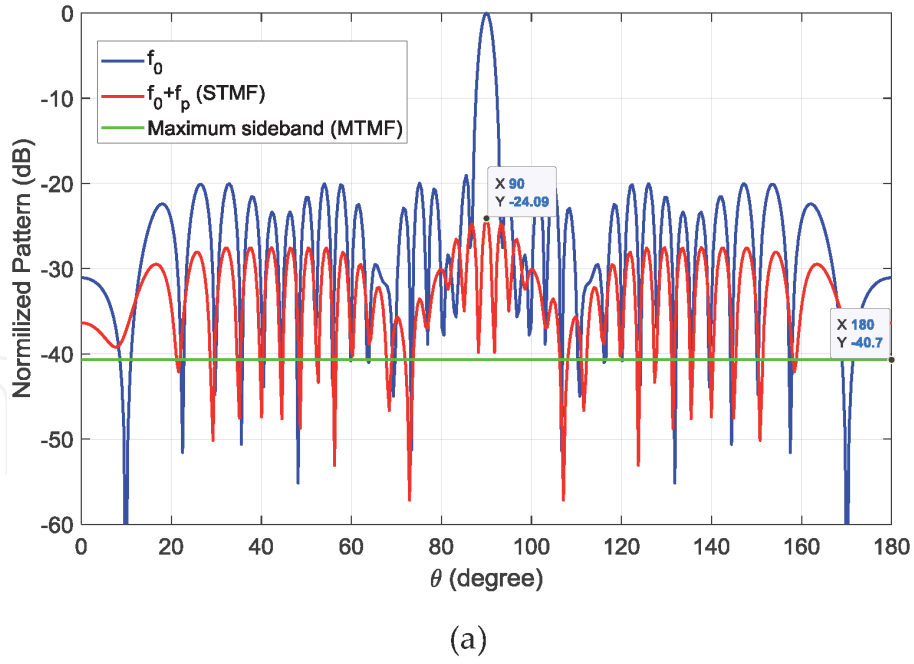**Figure 18.**
The optimized TMLA by the DE algorithm where the desired SLL is −20 dB (d = 0.7λ). (a) Normalized array patterns. (b) Optimized switch-on time of each element.

comparison between the TMLA-STMF, the first sideband of STMF is also presented. Its maximum level is −24.09 dB.

3. Reducing SLLs and SBLs in TMLA

In this section, an analytical method is used to minimize the SLLs and SBLs in TMLA [18]. The array pattern of the TMLA can be written in the following forms: For an odd number of elements $N = 2M + 1$ and $z_n = nd$, then

$$AF_0(\psi, t) = e^{j2\pi f_0 t} \sum_{n=-M}^{M} \tau_n e^{jn\psi} = e^{j2\pi f_0 t} \left(\tau_0 + \sum_{n=1}^{M} \left(\tau_{-n} e^{-jn\psi} + \tau_n e^{jn\psi} \right) \right) \quad (55)$$

where $\psi = kd \cos{(\theta)}$ and by assuming symmetrical excitations $\tau_n = \tau_{-n}$, then

$$AF_0(\psi, t, \tau) = e^{j2\pi f_0 t}\left(\tau_0 + 2\sum_{n=1}^{M}\tau_n \cos{(n\psi)}\right) \qquad (56)$$

Note that $\tau = [\tau_0, \tau_1, \dots, \tau_M]$ is a row vector that wants to be determined to satisfy the desired specifications (SLL, SBL, and directivity), where $\tau \in [0, 1]^M$. We should indicate that $\cos{(n\psi)}$ can be written as

$$\cos{(n\psi)} = T_n(\cos{(\psi)}) \qquad (57)$$

where T_n is the first kind Chebyshev polynomial of degree n. The sidelobes' locations of the fundamental array factor AF_0 can be determined by solving the equation $\partial AF_0/\partial\psi = 0$, where

$$\frac{\partial AF_0}{\partial\psi} = -2\sin{(\psi)}e^{j2\pi f_0 t}\sum_{n=1}^{M}n\tau_n U_{n-1}(\cos{(\psi)}) \qquad (58)$$

where U_{n-1} is the second kind Chebyshev polynomial and it has a relation with first kind Chebyshev polynomial

$$\frac{dT_n(s)}{ds} = nU_{n-1}(s) \qquad (59)$$

where

$$\begin{cases} U_0(s) = 1, U_1(s) = 2s \\ U_n(s) = 2sU_{n-1}(s) - U_{n-2}(s), n = 2, 3, \dots \end{cases} \qquad (60)$$

The sidelobes are located at $\psi_0 = \pi$ and $\psi_i = \arccos{(s_i)}$, where s_i are the roots of the following polynomial:

$$P_{\text{odd}}(s) = \sum_{n=1}^{M}n\tau_n U_{n-1}(s) \qquad (61)$$

By obtaining the roots s_i, in the region $[-1, 1]$, of the polynomial $P_{\text{odd}}(s)$ in terms of the excitation coefficients τ_n and substituting $\psi_i(\tau_1, \tau_2, \dots \tau_M) = \arccos{(s_i)}$ into (56), we get the following:

$$AF_0(\psi_i, t, \tau) = e^{j2\pi f_0 t}\left(\tau_0 + 2\sum_{n=1}^{M}\tau_n T_n(s_i(\tau_1, \tau_2, \dots \tau_M))\right) \qquad (62)$$

where $\text{SLL}_i = |AF_0(\psi_i, t, \tau)|$ is the SLL of the sidelobe located at ψ_i.

For an even number of elements $N = 2M$ and $z_{\pm n} = \pm(2n-1)d/2$, then

$$AF_0\left(\psi, t, \tau^{(1)}\right) = 2e^{j2\pi f_0 t}\sum_{n=1}^{M}\tau_n \cos{\left(\left(n - \frac{1}{2}\right)\psi\right)} \qquad (63)$$

where $\tau^{(1)} = [\tau_1, \tau_2, \dots, \tau_M]$.

The Chebyshev of 3rd and 4th kinds are given as

$$V_n(s) = \cos\left(\left(n + \frac{1}{2}\right)\psi\right) / \cos\left(\frac{\psi}{2}\right) \tag{64}$$

$$W_n(s) = \cos\left(\left(n + \frac{1}{2}\right)\psi\right) / \sin\left(\frac{\psi}{2}\right) \tag{65}$$

respectively, where $s = \cos\psi$.

The expression $AF_0(\psi, t, \boldsymbol{\tau}^{(1)})$ and $\partial AF_0 / \partial\psi$ can be written in terms of (64) and (65), respectively, as

$$AF_0\left(\psi, t, \boldsymbol{\tau}^{(1)}\right) = 2\cos\left(\frac{\psi}{2}\right) e^{j2\pi f_0 t} \sum_{n=1}^{M} \tau_n V_{n-1}(\cos(\psi)) \tag{66}$$

$$\frac{\partial AF_0}{\partial\psi} = -2\sin\left(\frac{\psi}{2}\right) e^{j2\pi f_0 t} \sum_{n=1}^{M} \left(n - \frac{1}{2}\right) \tau_n W_{n-1}(\cos(\psi)) \tag{67}$$

As described before, the sidelobes are located at $\psi_i = \arccos(s_i)$, where s_i are the roots, that are located in the region $[-1, 1]$ of the following polynomial:

$$P_{\text{even}}(s) = \sum_{n=1}^{M} \left(n - \frac{1}{2}\right) \tau_n W_{n-1}(s) \tag{68}$$

and the SLLs are given as

$$\text{SLL}_i = \left|AF_0\left(\psi_i, t, \boldsymbol{\tau}^{(1)}\right)\right| = \left|2\cos\left(\frac{\psi_i}{2}\right) \sum_{n=1}^{M} \tau_n V_{n-1}(s_i(\tau_1, \tau_2, \dots \tau_M))\right| \tag{69}$$

It should be indicated that there are no sidelobes contributed by the factor $\sin(\psi/2)$ since its roots are $\pm 2\pi$, which are a worthy advantage in designing even number of elements in TMLA.
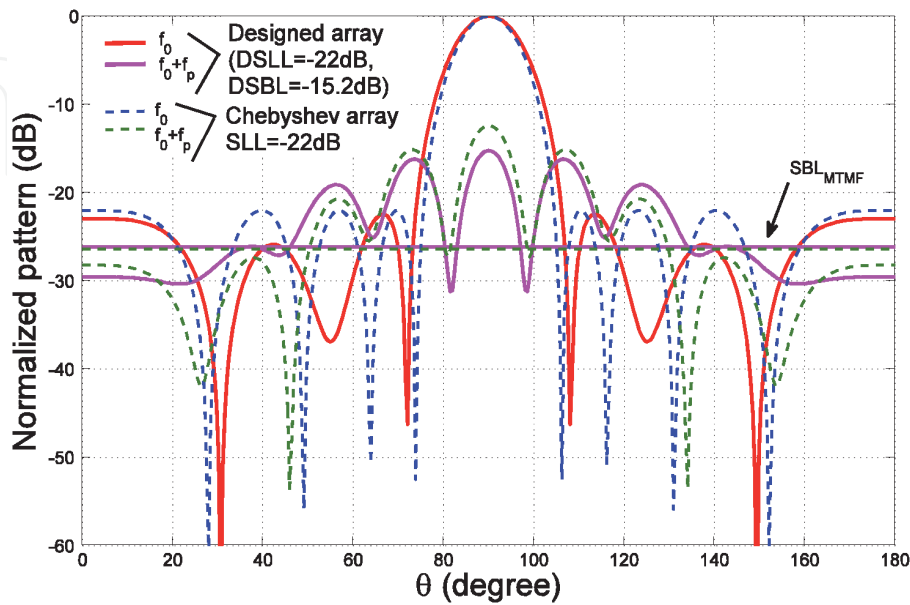

Figure 19.
The designed array $(N = 9, \text{DSLL} = -22 \text{ dB}, \text{DSBL}_{\text{STMF}} = -15.2)$ *and Chebyshev array* $(N = 9, \text{SLL} = -22\text{dB})$.
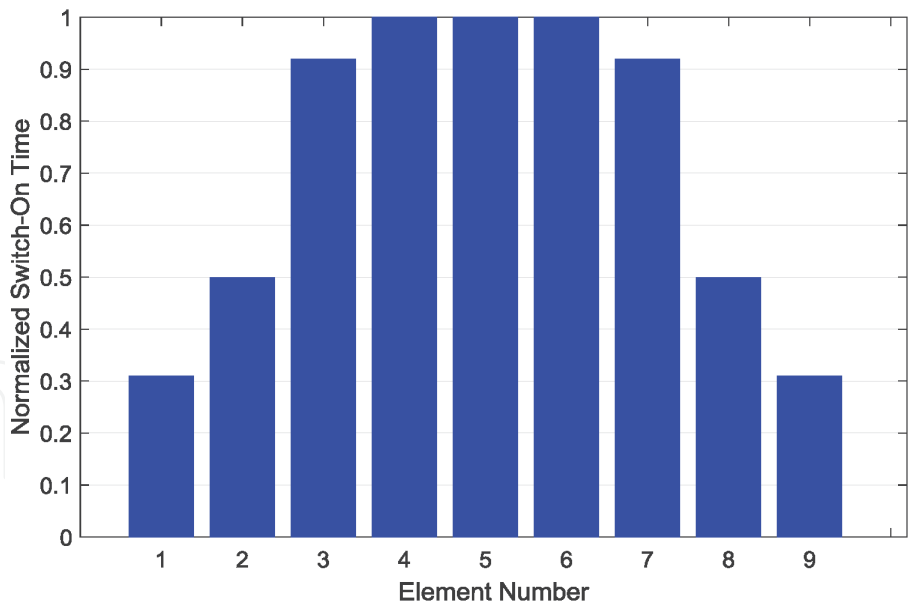
Figure 20.
Designed time sequence distributions of each antenna array element for $N = 9$, DSLL $=$
-22 dB, $DSBL_{STMF} = -15.2$.

Now let's design TMLA with nine elements to satisfy the specifications; DSLL $=$ -22 dB and $DSBL_{STMF} = -15.2$. In this case, the SBL for MTMF is -26.15 and the maximum directivity that can be achieved is $D_{max} = 16.2$ dB. The results are plotted in **Figures 19** and **20**. To investigate the effectiveness of the proposed method, a comparison is performed with nine-element Chebyshev array that has SLL equal to -22 dB. It has SBL equal to -12.4 and its directivity 16.42 dB which is larger than the designed array only with 0.22 dB. Note that $\xi_{on,n} = 0$ for all the cases.

Finally, it should be indicted that the TMLA can be designed by only controlling the time sequence distributions which is a very good advantage as compared to the conventional array under the following reasons:

1. Attain high accuracy in the designed array pattern in the TMLA because the switching distributions can be controlled at very high accuracy.

2. In the conventional array, attenuators and distributors are needed for exciting the array which is not accurate method. Therefore, it causes deviation in the designed array pattern and high SLLs are generated.

4. Conclusion

In this chapter, the main backgrounds and theories of TMLA are derived where different simulation examples are presented and discussed in detail. A comparison between different results given in the previous literature is also discussed. In addition, an analytical method to reduce the SLLs and SBLs in TMLA with maximum achievable directivity has been developed. This analytical method helps us to visualize the relation between switch-on durations, SLL, and SBL, which is an advantage compared to the other designing methods. It was shown that the TMLA has better performance than the conventional array.

Author details

Oussama Gassab[1,2]*, Arab Azrar[1] and Sara Bouguerra[1]

1 The Signals and Systems Research Laboratory, Department of Electronic, Institute of Electrical and Electronics Engineering (IGEE), University M'Hamed Bougara of Boumerdes, Boumerdes, Algeria

2 Key Lab of Ministry of Education for the Design and Electromagnetic Compatibility of High-Speed Electronic Systems, The Center for Microwave and RF Technologies (CMRFT), Shanghai Jiao Tong University, Shanghai, China

*Address all correspondence to: oussamagassab@yahoo.com

IntechOpen

References

[1] Ares-Pena FJ, Rodriguez-Gonzalez JA, Villanueva-Lopez E, Rengarajan SR. Genetic algorithms in the design and optimization of antenna array patterns. IEEE Transactions on Antennas and Propagation. March 1999;**47**(3):506-510

[2] Khodier MM, Christodoulou CG. Linear array geometry synthesis with minimum sidelobe level and null control using particle swarm optimization. IEEE Transactions on Antennas and Propagation. August 2005;**53**(8):2674-2679

[3] Gassab O, Azrar A. Novel mathematical formulation of the antenna array factor for side lobe level reduction. ACES Journal. 2016;**31**(12): 1452-1462

[4] Schrank H. Low sidelobe phased array antennas. IEEE Antennas and Propagation Society Newsletters. April 1983;**25**(2):4-9

[5] Shanks HE, Bickmore RW. Four-dimensional electromagnetic radiators. Canadian Journal of Physics. 1959;**37**(3): 263-275

[6] Kummer W, Villeneuve A, Fong T, Terrio F. Ultra-low sidelobes from time-modulated arrays. IEEE Transactions on Antennas and Propagation. 1963;**11**(6): 633-639

[7] Bregains JC, Fondevila-Gomez J, Franceschetti G, Ares F. Signal radiation and power losses of time-modulated arrays. IEEE Transactions on Antennas and Propagation. 2008;**56**(6):1799-1804

[8] Balanis CA. Time-varying and time-harmonic electromagnetic fields. In: Advanced Engineering Electromagnetics. 2nd ed. John Wiley & Sons; 2012, ch. 1. pp. 1-29

[9] Aksoy E, Afacan E. Calculation of sideband power radiation in time-modulated arrays with asymmetrically positioned pulses. IEEE Antennas and Wireless Propagation Letters. 2012;**11**: 133-136

[10] Zhu Q, Yang S, Yao R, Nie Z. Gain improvement in time-modulated linear arrays using SPDT switches. IEEE Antennas and Wireless Propagation Letters. Aug. 2012;**11**:994-997

[11] Yang S, Gan YB, Qing A. Sideband suppression in time-modulated linear arrays by the differential evolution algorithm. IEEE Antennas and Wireless Propagation Letters. 2002;**1**:173-175

[12] Yang S, Gan YB, Qing A, Tan PK. Design of a uniform amplitude time modulated linear array with optimized time sequences. IEEE Transactions on Antennas and Propagation. July 2005; **53**(7):2337-2339

[13] Poli L, Rocca P, Manica L, Massa A. Handling sideband radiations in time-modulated arrays through particle swarm optimization. IEEE Transactions on Antennas and Propagation. 2010; **58**(4):1408-1411

[14] Fondevila, Bregains, Ares, Moreno. Optimizing uniformly excited linear arrays through time modulation. IEEE Antennas and Wireless Propagation Letters. 2004;**3**:298-301

[15] He C, Yu H, Liang X, Geng J, Jin R. Sideband radiation level suppression in time-modulated array by nonuniform period modulation. IEEE Antennas and Wireless Propagation Letters. 2015;**14**: 606-609

[16] Guo J, Yang S, Chen Y, Rocca P, Hu J, Massa A. Efficient sideband suppression in 4-D antenna arrays through multiple time modulation frequencies. IEEE Transactions on Antennas and Propagation. 2017;**65**(12): 7063-7072

[17] Kanbaz I, Yesilyurt U, Aksoy E. A study on harmonic power calculation for nonuniform period linear time modulated arrays. IEEE Antennas and Wireless Propagation Letters. 2018; **17**(12):2369-2373

[18] Gassab O, Azrar A, Dahimene A, Bouguerra S. Efficient mathematical method to suppress sidelobes and sidebands in time-modulated linear arrays. IEEE Antennas and Wireless Propagation Letters. May 2019;**18**(5): 836-840